Solar Physics (2026) 301:29
https://doi.org/10.1007/s11207-026-02616-2

RESEARCH

Tracing the Solar Wind Cycle at 1 AU: Variability in the Delayed Response to Solar Activity

Raffaele Reda[1] · **Luca Giovannelli**[1] · **Tommaso Alberti**[2]

Received: 12 June 2025 / Accepted: 16 January 2026 / Published online: 18 February 2026

Abstract

The continuous flux of charged particles from the Sun, i.e., the solar wind, influences both planetary and circumplanetary environments. Although the precise origin of each type is still debated, the solar wind originates primarily from the expansion of the solar corona and is driven by the solar magnetic field. The cyclic 11-year variations observable in several solar activity proxies can also be traced in the average properties of the solar wind, though the relationship in terms of amplitude and phase synchronization with solar activity is not uniform. Focusing on the period 1965 – 2024, we investigate how the relationship between a chromospheric proxy, the Ca II K index, and 1AU solar wind properties, such as speed, temperature, and dynamic pressure, has evolved over the last five solar cycles. On the one hand, variations in their relationship are found in terms of time lag, correlation coefficient, and amplitude (i.e., fit slope) in a cycle-based analysis. In particular, we find evidence consistent with a linear relationship between the time lag (in years) and the slope of the fit characterizing the dependence of solar wind properties on the intensity of the solar magnetic cycle. We also examine these variations in light of the contribution of the different solar wind flow types along individual solar cycles. On the other hand, continuous cross-correlation reveals distinct dynamical regimes in solar wind–Ca II K lag, with stable behavior at 2 – 4 years and instability emerging at both shorter and longer lag intervals, suggesting a nonlinear bifurcation mechanism. Finally, the cycle-to-cycle variations reported can help in understanding the space climate connection between solar activity and near-Earth solar wind properties, additionally providing insight into the contribution of each solar wind flow type.

Keywords Space climate · Solar wind · Ca II K index · Solar cycle · Time lag

✉ R. Reda
raffaele.reda@roma2.infn.it

L. Giovannelli
luca.giovannelli@roma2.infn.it

T. Alberti
tommaso.alberti@ingv.it

1 Department of Physics, University of Rome Tor Vergata, via della Ricerca Scientifica 1, Rome, 00133, Italy

2 Istituto Nazionale di Geofisica e Vulcanologia, via di Vigna Murata 605, 00143, Rome, Italy

1. Introduction

The Sun is a dynamic star whose varying magnetic activity and related phenomena permeate and modify the whole heliosphere. The dynamo processes at the core of this activity exhibit variability over a wide range of timescales (e.g., Hathaway 2010; Vecchio et al. 2017; Beer, Tobias, and Weiss 2018; Usoskin 2023), encompassing the two main recognized periodicities of solar activity: solar rotation and the 11-year cycle. Many phenomena are related to solar activity, with flares, coronal mass ejections, solar energetic particle flux, and solar wind being the main ones. Periodicities in solar wind parameters have also been studied, revealing several scales of variation, from a few minutes to decadal timescales (e.g., Katsavrias, Preka-Papadema, and Moussas 2012; Li, Zhang, and Feng 2017; Reda, Giovannelli, and Alberti 2024). Of particular interest is the long-term variability of the solar wind. Although several solar wind models have been implemented (see e.g., Reiss et al. 2019; Hazra et al. 2021; Perri et al. 2022), predictions on long-term scales remain challenging. Changes in solar wind conditions over solar cycles can have profound effects on the heliospheric environment, including modulation of galactic cosmic rays, variations in the structure of the heliospheric current sheet and long-term trend in geomagnetic activity. Studying these variations is critical for understanding solar-terrestrial interactions and for developing models that can reliably predict space climate conditions over extended periods.

Among the time scales of variations, it is widely recognized that various solar wind parameters (e.g., speed, temperature, dynamic pressure) exhibit periodicity similar to that of the Schwabe cycle (approximately 11 years), to the extent that it has often been referred to as the *'solar wind cycle'* (El-Borie 2002; Katsavrias, Preka-Papadema, and Moussas 2012; Li, Zhang, and Feng 2017; Reda, Giovannelli, and Alberti 2023; Reda et al. 2024). However, it has been shown that the two cycles are not in phase, with evidence of a time lag — with an average value of ~ 3 years — relative to various solar activity proxies obtained through the use of multiple techniques (Köhnlein 1996; Samsonov et al. 2019; Reda et al. 2023; Reda, Giovannelli, and Alberti 2024). Reda et al. (2024) provide evidence of information flow from solar activity (specifically Ca II K) to solar wind speed and dynamic pressure, indicating more than just a simple peak-to-peak correlation. Although general patterns can be observed, the specific phase difference between the solar wind and solar activity varies over time, with occurrences of anti-phase and quadrature states when focusing on solar cycle timescales, as recently reported by Reda, Giovannelli, and Alberti (2024). The presence of a time delay in the response of 1 AU solar wind properties to solar activity is not coincidental. Indeed, Carbone et al. (2024) recently demonstrated theoretically that it arises naturally from a modified Parker solar wind model, in which the effect of the solar magnetic cycle is introduced using a modified Van der Pol non-linear oscillator. Efforts have been made to understand the physics of the coupling between the dynamo and the solar wind (Pinto et al. 2011; Dash, Nandy, and Usoskin 2023), also focusing on a more general stellar context where the presence of a feedback loop between a stellar activity cycle and its related stellar wind has also been reported by Perri et al. (2021).

While previous studies have focused on estimating a global time lag or analyzing the instantaneous phase difference between solar activity and solar wind parameters, our approach introduces a cycle-resolved perspective. Specifically, we segment the time series into individual solar cycles and perform a re-phasing of the signals to align them within each cycle. This allows us to examine the correlations between the Ca II K index and various solar wind parameters on a cycle-by-cycle basis. Following this re-phasing, we analyze the linear correlations for each cycle and investigate whether the slopes of these correlations exhibit a systematic relationship with the corresponding time lag. This approach removes cycle-to-cycle variations, enhancing the linearity of the relationships within each cycle. It also

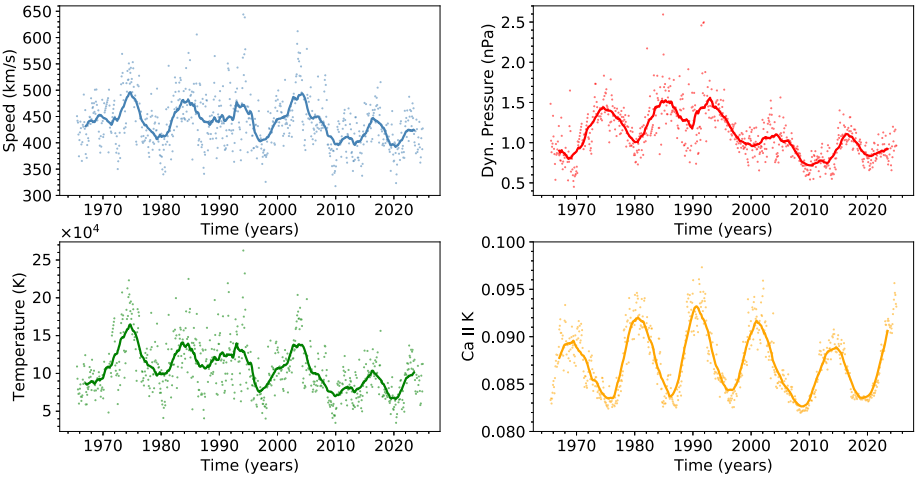

Figure 1 Monthly averages (points) and 37-month sliding window averages (lines) of solar wind speed (top left), solar wind dynamic pressure (top right), solar wind temperature (bottom left) and Ca II K index (bottom right). For the period from November 2017 to December 2024 the Ca II K index was reconstructed using the Mg II index.

provides a framework for better understanding how the timing and intensity of solar forcing impact heliospheric conditions across different solar cycles.

Therefore, this study investigates the space-climate relationship between the Ca II K index and OMNI 1 AU solar wind properties over five solar cycles. Using a cross-correlation approach, we analyze the temporal evolution of their relative time lag, correlation strength and fit slope, with a particular focus on variations over solar-cycle-length time windows. Furthermore, this study extends the analysis of continuous variations in the lag, aiming to highlight possible multiple equilibrium states in the parameter space. Moreover, we investigate the time lag of the solar wind decomposed in three main components (CME-, Corotating-stream- and Slow-wind related) to give a possible explanation of the phenomena.

2. Dataset

The solar wind data employed in this work are 1AU OMNI combined, definitive, hourly interplanetary plasma (IP) data, time-shifted to the nose of the Earth's Bow Shock (King and Papitashvili 2005), accessed on March 1, 2025.[1] In particular, we use the following parameters at 1 AU: IP proton temperature (T), IP ion number density (n_i) and IP flow speed (v). All solar wind parameters are then re-binned to obtain monthly averages. By combining density and speed, we calculate also the dynamic pressure, defined as $P_{dyn} = \frac{1}{2} m_p n_i v^2$, with the proton mass m_p assumed to be the ion mass. The dynamic pressure of the solar wind is a relevant parameter since it is the main one which controls the extension of Earth's magnetosphere.

The solar proxy we use here is the Ca II K 0.1-nm emission index,[2] obtained by combining data from the Kodaikanal Solar Observatory, the National Solar Observatory (NSO) at

[1] https://omniweb.gsfc.nasa.gov.

[2] https://solis.nso.edu/0/iss/.

Table 1 Solar cycle durations reported by SIDC-SILSO.

Solar cycle	Starting time	Ending time
20	October 1964	February 1976
21	March 1976	August 1986
22	September 1986	July 1996
23	August 1996	November 2008
24	December 2008	November 2019
25	December 2019	ongoing

Sacramento Peak, and the Synoptic Optical Long-term Investigations of the Sun (SOLIS). The procedure used to obtain this composite, as well as details about the dataset, are described in Bertello et al. (2016). Although this composite contains monthly averaged data up to November 2017, we extend it to the end of 2024 by using the relation with the Mg II index presented by Reda and Penza (2024), which is calibrated on the last four solar cycles. To this scope, we use the Mg II index composite provided by the University of Bremen.[3] The use of the Ca II K index as a proxy for solar activity is preferred over the Sunspot Number (SSN) because it provides a physical measure of solar chromospheric emission. Unlike the SSN, which represents a synthetic measure of solar activity (see e.g., Usoskin 2023), the Ca II K index directly reflects spectral variations and is less biased by the presence of concentrated magnetic structures on the solar surface. Previous studies have demonstrated that it reliably traces the strength of the solar magnetic field across all phases of the solar cycle, even during intervals of low activity or the absence of sunspots, such as solar minima (Pevtsov et al. 2016; Kahil, Riethmüller, and Solanki 2017). However, the solar emission in the Ca II lines has been demonstrated to be strongly correlated with the SSN, both when considering the combined H & K emission (Ferreira et al. 2024) and the emission in the individual K line (Bertello et al. 2016). Moreover, the emission in the Ca II K line has long been monitored in stars other than the Sun, giving this work a potentially broader stellar perspective.

Although Ca II K data start from the beginning of 1900, solar wind data only begin in the 1960s, with simultaneous speed, density, and temperature data available since 1965. Thus, we consider here the overlapping time period from July 1965 to December 2024, which covers the majority of Solar Cycle 20, the entire Cycles 21 – 22 – 23 – 24 and the rising phase of cycle 25. The start and end times of each cycle, as reported by SIDC-SILSO, is reported in Table 1.

As a final step, to study the solar activity–solar wind relationship and how it varies across the solar cycles, we adopt a space climate approach, following the methodology of Köhnlein (1996), by smoothing the data with a 37-month sliding window average. This procedure acts as a low-pass filter, removing short-term variability that is not of interest in the context of this study. The same approach has been applied to the same dataset in earlier works (see e.g., Reda et al. 2023; Reda, Giovannelli, and Alberti 2023). Figure 1 shows the monthly averages and the respective smoothing for the relevant parameters studied in the next section.

[3] http://www.iup.uni-bremen.de/UVSAT/Datasets/mgii.

3. Relationship on Space Climate Scales

3.1. Cycle-to-Cycle Relationship

We study the relationship between the Ca II K index and solar wind parameters, with a particular focus on how this relationship changes from cycle to cycle. This relationship is examined using cross-correlation analysis, which quantifies the degree of similarity between two time series as a function of the relative displacement (i.e., time lag) of one with respect to the other. Given two discrete time series $x(t)$ and $y(t)$, the cross-correlation between them is defined as

$$R_{xy}(\tau) = \sum_{\tau=-\infty}^{+\infty} x^*(t)\, y(t+\tau) \tag{1}$$

where $x^*(t)$ denotes the complex conjugate of $x(t)$ and the variable τ is the time lag (or delay) between the two time series.

We consider here only Solar Cycles 20 to 24. We exclude the rising phase of Cycle 25 because the cross-correlation analysis relies on the synchronization of the peaks in the time series. Therefore, to obtain significant results, the peaks of each time series must be included. Since the peak associated with Cycle 25 is not clearly identifiable in all time series (see Figure 1), we decided to exclude the rising phase of this cycle from the present analysis. For each cycle, we perform a cross-correlation analysis between the Ca II K index and three solar wind parameters (i.e., speed, dynamic pressure, and temperature) identifying the time lag τ that maximizes the cross-correlation function R_{xy}. In particular, we consider only positive time lags of the solar wind parameters with respect to the Ca II K index, under the assumption of a causal relationship in which variations in solar activity precede and potentially influence the solar wind behavior. Once the time lag for each solar cycle and for each solar wind parameter relative to the Ca II K index is identified, we analyze their relationships by back-shifting the corresponding solar wind quantity. The scatter plots in Figure 2 illustrate the cycle-to-cycle correlations, with each color representing a different solar cycle. These relationships are shown between the Ca II K index and solar wind speed (top), dynamic pressure (middle), and temperature (bottom). A clear linear correlation emerges within each solar cycle when the appropriate time lag is taken into account. A detailed overview of the key statistical parameters of the relationships is provided in Table 2, Table 3, and Table 4, respectively, where we report the time lag, Pearson correlation coefficient, and p-value for each solar cycle. Additionally, we include the coefficients of the linear regression fits shown in Figure 2, which are in the form

$$\xi_{sw} = (\alpha \pm \Delta\alpha)\, CaIIK + (\beta \pm \Delta\beta), \tag{2}$$

where ξ_{sw} represents one of the solar wind parameters, α is the slope of the fit and β is the intercept. The p-values of the correlation are computed by accounting for autocorrelation in both time series. In particular, we use the effective sample size as the degrees of freedom, employing the following formula by Zwiers and von Storch (1995):

$$n_{eff} = \frac{n}{1 + 2\sum_{\tau=1}^{L}(1 - \frac{\tau}{n})\, r(\tau)}. \tag{3}$$

Here, τ represents the time lag of the autocorrelation, and $r(\tau)$ is the corresponding correlation coefficient. We account for autocorrelation up to a truncation lag $L = \sqrt{n}$, where

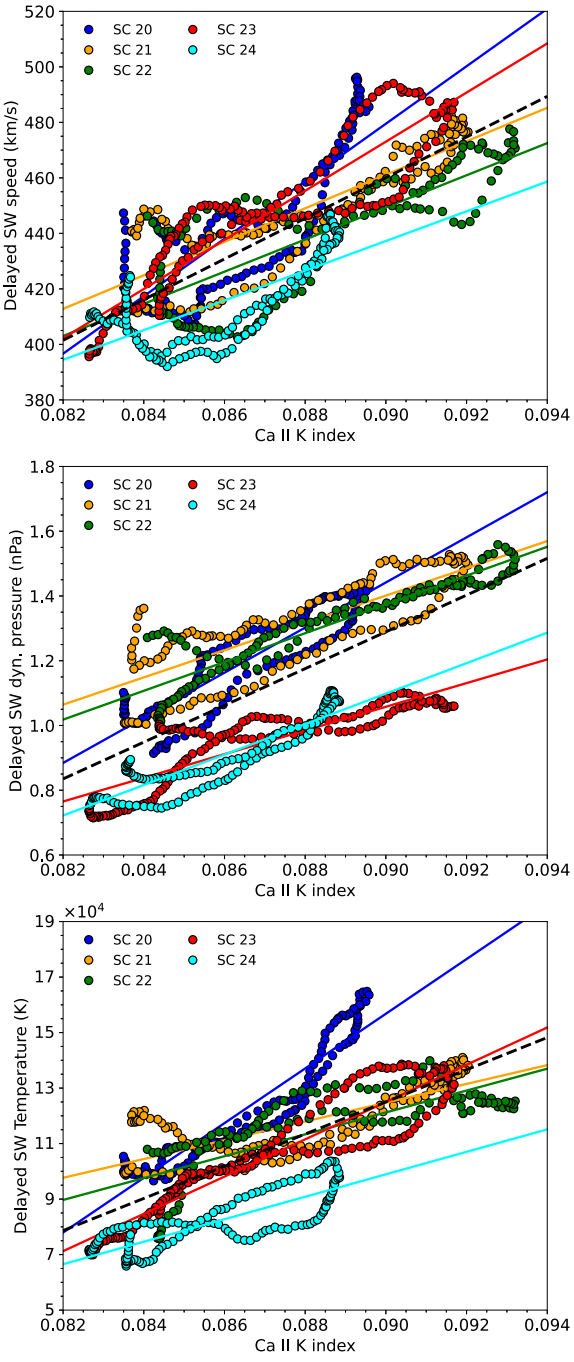

Figure 2 Scatter plots showing the cycle-to-cycle correlation of delayed solar wind speed (top panel), delayed solar wind dynamic pressure (middle panel) and delayed solar wind temperature (bottom panel) with Ca II K index. Each color is representative of a Solar Cycle from 20 to 24, as explained in the legend. The best regression fit for each cycle is shown with the corresponding color line. The black dashed line represents the best regression fit obtained considering all the data points.

n is the size of the time series considered. For statistical significance, we compare with a p-value of 0.05.

Table 2 Cycle-to-cycle correlation between Ca II K index and solar wind speed. Column 1: Solar cycle number; Column 2: Pearson's correlation coefficient; Column 3: P-value corresponding to the correlation; Column 4: Time lag in years; Columns 5 and 6: Linear regression fit parameters.

Solar cycle	Corr. Coeff.	p-value	Time Lag (yr)	Fit Slope ($\times 10^2$ km s^{-1})	Fit Intercept($\times 10$ km s^{-1})
20	0.83	0.025	5.8	104 ± 6	-45 ± 5
21	0.85	0.025	3.5	60 ± 3	-8 ± 3
22	0.79	0.042	2.6	58 ± 4	-7 ± 4
23	0.92	0.004	1.8	88 ± 3	-30 ± 3
24	0.71	0.076	2.7	54 ± 5	-4 ± 4
All	0.78	$4.26 \cdot 10^{-4}$	3.3	73 ± 2	-20 ± 2

Table 3 Same as Table 2, but for the correlation between Ca II K index and solar wind dynamic pressure.

Solar cycle	Corr. Coeff.	p-value	Time Lag (yr)	Fit Slope (nPa)	Fit Intercept (nPa)
20	0.91	0.006	5.3	69.7 ± 2.8	-4.83 ± 0.24
21	0.81	0.040	3.9	42.1 ± 2.7	-2.39 ± 0.24
22	0.93	0.005	1.9	44.5 ± 1.7	-2.63 ± 0.15
23	0.86	0.019	2.1	36.6 ± 1.8	-2.23 ± 0.15
24	0.89	0.010	2.5	47.1 ± 2.1	-3.14 ± 0.18
All	0.71	$7.27 \cdot 10^{-7}$	3.1	56.8 ± 2.2	-3.82 ± 0.19

Table 4 Same as Table 2, but for the correlation between Ca II K index and solar wind temperature.

Solar cycle	Corr. Coeff.	p-value	Time Lag (yr)	Fit Slope ($\times 10^5$ K)	Fit Intercept ($\times 10^4$ K)
20	0.95	0.002	5.3	99 ± 3	-73 ± 2
21	0.77	0.053	3.3	34 ± 2	-18 ± 2
22	0.76	0.058	0.7	39 ± 3	-23 ± 3
23	0.94	0.003	1.5	67 ± 2	-48 ± 2
24	0.81	0.030	1.3	41 ± 3	-27 ± 2
All	0.72	$2.21 \cdot 10^{-5}$	2.4	58 ± 2	-40 ± 2

The correlation between the Ca II K index and solar wind speed (Table 2) is strong across all solar cycles, with Pearson correlation coefficients ranging from 0.71 (Cycle 24) to 0.92 (Cycle 23). The statistical significance of the correlations is confirmed by the associated p-values, which are below 0.05, except for solar Cycle 24. A notable feature is the decrease in time lag from 5.8 years in Cycle 20 to 1.8 years in Cycle 23, followed by a slight increase in Cycle 24. While the correlation remains consistently high across all solar cycles, the slope of the linear regression also shows significant variation, with steeper slopes in Cycles 20 and 23, whereas shallower slopes are found in Cycles 21, 22 and 24.

For the dynamic pressure (Table 3) the correlation is even stronger. Indeed, the Pearson coefficient ranges from 0.81 (Cycle 21) to 0.93 (Cycle 22), with all p-values being consistently below the reference value 0.05, confirming the statistical significance of the correlations. Similar to what is observed for the solar wind speed, the time lag of solar wind dynamic pressure relative to Ca II K decreases from the 5.3 years of Cycle 20 to the 1.9

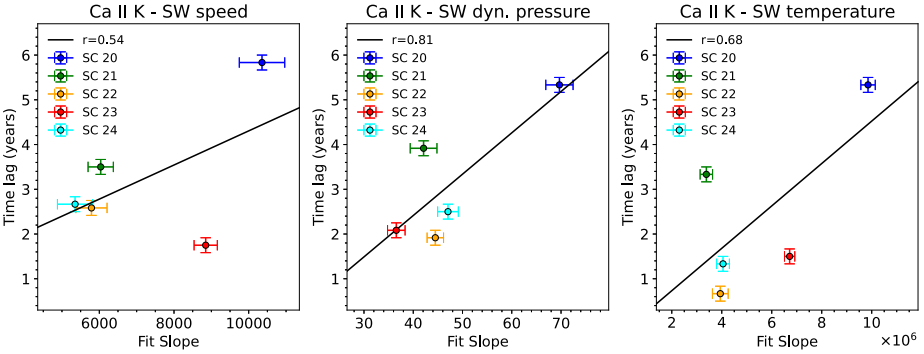

Figure 3 Cycle-to-cycle dependence of the time lag as a function of the fit slope. The scatter plots show the results for solar wind speed (left), solar wind dynamic pressure (center), and solar wind temperature (right). The solid black line represents the best fit over the five cycles.

years of Cycle 22, followed by a small increase in the subsequent two cycles. The slope of the linear regression shows moderate variation across the cycles, with Cycle 20 having the steepest one.

The correlation between Ca II K index and solar wind temperature (Table 4) is consistently high across all cycles, indicating a strong positive relationship between the two parameters. Specifically, Cycles 20 and 23 show the strongest correlations, with coefficients of 0.95 and 0.94, respectively, and very low p-values, confirming the statistical significance of the results. In contrast, although the correlations for Cycles 21 and 22 remain substantial, their corresponding p-values slightly exceed the 0.05 value, being 0.053 and 0.058, respectively. The time lags vary among cycles, ranging from 0.7 years (Cycle 22) to 5.3 years (Cycle 20), with shorter lags observed in the more recent cycles. Also for the temperature, the steepest slope is observed in Cycle 20. It is interesting to note that, in general, higher values of the fit slope are associated with higher correlation coefficients, with the steepest slopes for all parameters observed during Cycle 20. This suggests a stronger sensitivity of the solar wind properties to variations in the Ca II K index during this cycle. Considering that Cycle 20 also exhibits the longest time lag for all parameters, we further investigated a possible relationship between the time lag and the fit slope. Figure 3 shows the relationship for Cycle 20 to Cycle 24. There is a possible indication of a linear trend between the time lag and the fit slope, particularly for dynamic pressure and temperature (middle and right panels), while it appears less pronounced for speed. Although a statistical claim of correlation between the two quantities cannot be made based on only five data points, this result relies on all currently available solar wind data. Nevertheless, further statistical confirmation with the accumulation of new data in the coming years will be necessary to assess the significance of this indicative finding.

3.2. Relationship with Continuous Windowing

In the previous subsection, we investigated the relationship between solar wind parameters and the Ca II K index, focusing primarily on the time lag and its cycle-to-cycle changes. Here, we take a step further by analyzing the variations in time lag in a more continuous way. The approach is the same as in Section 3.1, based on cross-correlation analysis. We still consider 11-year windows, however, in this case, they are not strictly aligned with individual solar cycles. As before, for each window we perform a cross-correlation analysis and

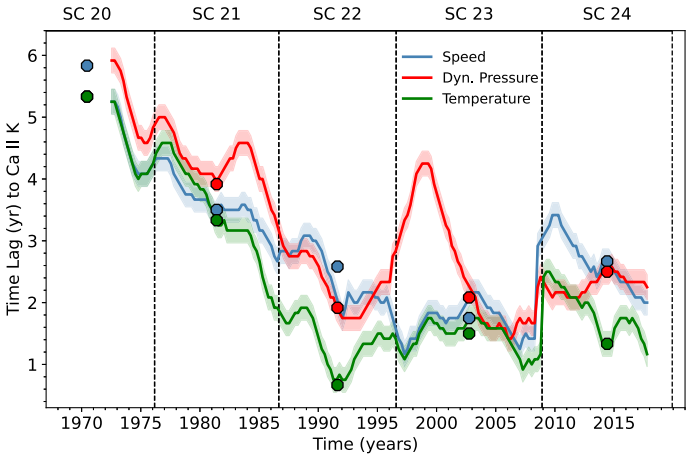

Figure 4 Relative time lag of the solar wind parameters with respect to Ca II K, obtained using an 11-year sliding window. Vertical lines are used to denote each solar cycle. The points, placed at the center of each solar cycle window, represent the average time lag for each cycle, as reported in Tables 2, 3, and 4. Note that for Solar Cycle 20 the green and red points are superimposed.

extract the time lag corresponding to the maximum correlation coefficient, along with the value of that coefficient. Figure 4 shows the relative time lag of the solar wind parameters (speed, dynamic pressure, and temperature) with respect to the Ca II K index, as determined using the 11-year sliding window. The time lags of the solar wind signals are all computed relative to the Ca II K index, as it is used as a reference clock for the solar magnetic cycle. By shifting the window in 3-month steps, we obtain a detailed view of how the time lag evolves over time. To compare these results with the time lags obtained for each cycle in Section 3.1, as detailed in Tables 2, 3, and 4, we place a point at the center of the corresponding solar cycle window. The trends in speed and temperature appear to be very similar, whereas larger differences are observed in the time lag of the solar wind dynamic pressure, with the presence of a sudden increase of the time lag at the beginning of Cycle 23. This marked increase has also been reported by Reda, Giovannelli, and Alberti (2024) (see their Figure 4), where it is clearly visible in terms of phase difference between the Ca II K index and the solar wind dynamic pressure when focusing on solar cycle time scales. Figure 4 further highlights the variability of the time lag, giving evidence of a sharp decrease during Cycles 20 and 21, followed by more moderate variations thereafter, except in the case of dynamic pressure. This is consistent with the existence of multiple equilibrium states in the time lag, as proposed by Reda, Giovannelli, and Alberti (2024), who reported the occurrence of anti-phase and quadrature states in the phase difference (or, equivalently, in the time lag) between the Ca II K index and solar wind properties across solar-cycle timescales.

Taking advantage of the features obtained with the analysis on the 11-year sliding window, Figure 5 illustrates a 3D scatter plot depicting the relationship between the time lag of the solar wind dynamic pressure with respect to Ca II K index, the Ca II K index itself and time. Each point represents a value derived from an 11-year sliding window. The color of the points reflects the correlation coefficient between the dynamic pressure and the Ca II K index within the corresponding window. Here, we show only the case of the Ca II K index with the solar wind dynamic pressure, but similar behavior is observed when considering the solar wind speed or temperature (not shown). This visualization allows us to examine how the time lag and the strength of the correlation evolve in relation to both solar activity

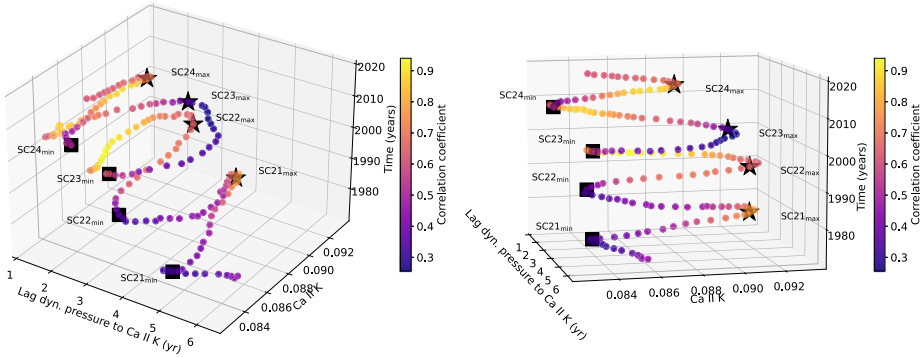

Figure 5 3D visualizations, from two different perspectives, of the relationship between the relative time lag of solar wind dynamic pressure with respect to the Ca II K index, obtained using an 11-year sliding window, and the Ca II K index itself, as a function of time. The color map indicates the correlation coefficient within the reference 11-year window. Black stars mark the solar maxima, while black squares indicate the solar minima.

(as traced by the Ca II K index) and time. The presence of loops in the lag–Ca II K plane is well visible, where each loop can be linked to each solar cycle.

By inspecting the behavior of the correlation coefficient over each solar cycle in the 3D state-space described by the time lag, the Ca II K index and time, we can highlight the presence of distinct regimes, exhibiting different features. Specifically, when focusing on intermediate time lags (2 yr $\leq \tau \leq$ 4 yr) a periodic pattern, characterized by stronger correlations during solar maxima and weaker correlations during solar minima, is observed. We identify this state as a "stable" state. Conversely, no clear periodic behavior of the correlation coefficient is observed at both short ($\tau <$ 2 yr) and long ($\tau >$ 5 yr) lags, which we mark as the "unstable" state. Thus, we suggest the presence of a possible bifurcation process through which the system transitions between different stability states with different dependence of the time lags on the solar cycle phases. A more detailed interpretation of these results is provided in the discussion section.

3.3. Solar Wind Contribution from Different Flow Types

To further understand the cycle-to-cycle variations in the relationships between the Ca II K index and solar wind properties, both in terms of time lag and amplitude, we investigate the relative contribution of the different solar wind source regions over the different solar cycles. To this end, we use the dataset from Richardson (2023), previously presented in Richardson and Cane (2012), in which the authors classify the near-Earth solar wind into three flow types: (1) Corotating high-speed streams, fast flows originating primarily from coronal holes; (2) Coronal mass ejection (CME)-related flows, originating from CMEs and including interplanetary CMEs, shocks, and sheath regions; and, (3) Slow wind, typically associated with the streamer belt at the Sun. We first compute the monthly percentage of time during which each solar wind type was present, and then apply a 37-month sliding-window average to these fractions in order to match the temporal filtering of the Ca II K index and the solar wind parameter time series. Figure 6 shows a comparison between the Ca II K index and the percentage of time during which each solar wind source type was present over the past five solar cycles. It is evident that the CME-related contribution varies in phase with the solar cycle, exhibiting a pronounced peak that closely follows the maximum of the Ca II K index. This behavior reflects the enhanced occurrence of CMEs during

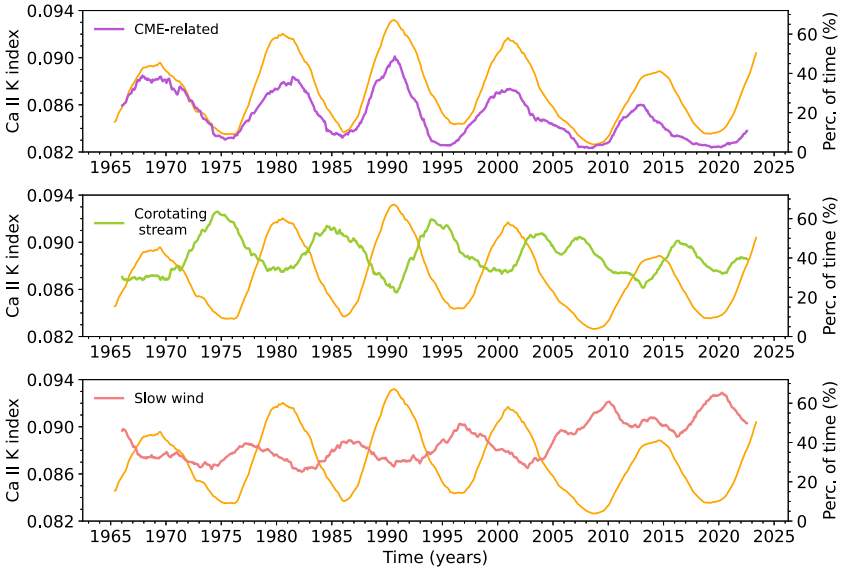

Figure 6 37-month moving averages of the Ca II K index (orange) and the percentage of time dominated by the different solar wind source types, as obtained from the dataset by Richardson (2023) CME-related (top), Corotating stream (middle) and Slow wind (bottom).

periods of high solar activity. The contribution from corotating streams is generally higher during the declining phase of the cycle and near solar cycle minimum, though its timing shows some differences across cycles. For instance, in Solar Cycle (SC) 20 the peak occurs very close to solar minimum, while in subsequent cycles it shifts toward the declining phase. The slow solar wind typically reaches its maximum around solar minimum, consistent with its association with the heliospheric plasma sheet and the streamer belt. An additional noteworthy feature is the marked increase in the fraction of slow wind-dominated time during the last two solar cycles, indicating an apparent long-term change in the global structure of the solar wind environment. At the same time the CME-related contribution decreases in a similar way in the last two solar cycles.

To relate the contribution of each solar wind type to the cycle-to-cycle variations in the time lag between the solar wind parameters and the Ca II K index, we perform a cross correlation analysis over individual cycles between the Ca II K index and the percentage of time associated with each of the three solar wind types within each solar wind cycle. As in Section 3.1, we identify the time lag that maximizes the cross-correlation function R_{xy}. The results are presented in the upper panel of Figure 7, where we compare the cycle-to-cycle time lags of corotating streams and slow wind relative to the Ca II K index with the corresponding lags of solar wind speed and dynamic pressure. We do not report the CME-related case, as its cross-correlation with the Ca II K index consistently peaks at zero time lag. The time lag associated with corotating streams shows a trend very similar to that observed for both the speed and dynamic pressure. A similar trend, although shifted toward higher values, is also observed for the slow wind, with a large time lag in SC 20, while during the last four cycles it is consistently in anti-phase with the Ca II K index ($\tau \sim 5.5$ yrs).

In the bottom panel of Figure 7, we also show the percentage of time for each solar wind type over each solar wind cycle. CME-related solar wind displays a steady decline

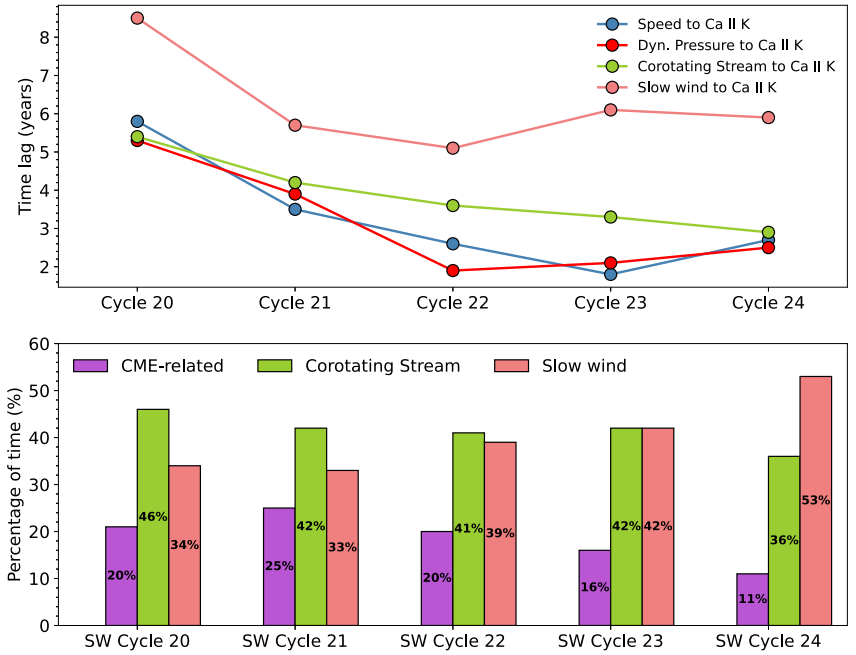

Figure 7 Top: Cycle-to-cycle variations in the time lag relative to the Ca II K index for solar wind speed, solar wind dynamic pressure, and the percentage of time dominated by Corotating streams and by Slow wind. Bottom: Percentage of time dominated by the different solar wind sources for each solar wind cycle.

across the last five cycles, decreasing from $\sim 20-25\%$ in SCs 20–21–22 to just $\sim 11\%$ in SC 24, indicating a progressively smaller contribution from transient CME outflows to the overall solar wind during the most recent cycles. Corotating streams remain comparatively stable across Cycles 20–23, contributing $\sim 41-46\%$, with only a modest reduction in SC 24 (down to 36%). This stability highlights the persistent role of coronal hole-associated streams as a major component of the solar wind over multiple decades. Slow wind, by contrast, shows a marked increase over time, rising from $\sim 34\%$ in SC 20 to become the dominant component in SC 24, reaching $\sim 53\%$. Overall, the results indicate a gradual transition from a mixed solar wind composition dominated by corotating streams to one increasingly characterized by slow wind in the most recent solar cycles, especially in SC 24 in which it is the dominant component.

4. Discussion and Conclusions

The results of this work support a strong correlation between the Ca II K index and the solar wind speed, dynamic pressure, and temperature when focusing on space climate time scales. By means of a cross-correlation analysis, we infer the time lag of the solar wind parameters with respect to the Ca II index for each of the last five solar cycles. We also extract other parameters connected to the correlation, such as fit slope and intercept, correlation coefficient and p-value. Although the relationship remains consistently strong, it exhibits cycle-to-cycle fluctuations in time lag, fit slope, and intercept. Evidence of a possible linear relationship between the cycle-to-cycle time lag and fit slope over each cycle is observed. Although it is

not possible to draw statistical inferences based on only five points (i.e., five solar cycles), this result encompasses the entire time interval for which in-situ solar wind measurements are available. Additional data will be required to establish its statistical significance. In their theoretical model, Carbone et al. (2024) identified a dependence of the time lag on the amplitude of the solar forcing (which is actually the Ca II K index in our case). In particular, they observed a tendency for the time lag to increase as the amplitude of the solar forcing decreases. Assuming a fixed value for the quantity ξ_{sw} in Eq. 2, a lower forcing amplitude corresponds to a steeper fit slope. This implies that the model-based result by Carbone et al. (2024) is consistent with the possible linear relationship observed here between the time lag and the fit slope. However, further investigations in this direction are certainly needed to confirm the result.

To understand the trend observed in the cycle-to-cycle time lag of the solar wind parameters relative to the Ca II K index, we examine the contributions of the CME-related, corotating-stream, and slow-wind components to the overall solar wind. The time lag associated with the corotating stream component shows a trend very similar to that observed for both the solar wind speed and dynamic pressure. This component dominates the solar wind composition during SCs 20 – 21 – 22 – 23, whereas in the more recent SC 24 the slow wind exhibits a marked increase, becoming the dominant contributor. In contrast, the CME-related component displays a significant decline, nearly halving its contribution from SC 20 to SC 24. The trend observed in the cycle-to-cycle time lag of the solar wind parameters, to a first approximation, reflects the behavior of the corotating stream component, which is the dominant contributor over SCs 20 – 23. On closer inspection, however, it emerges from a complex interplay among all solar wind components, including the CME-related and slow-wind flows, with these two components exhibiting opposite trends in their percentage contribution.

The decomposition of the solar wind in three main components opens to the possibility to interpret the variation of time lag between solar wind parameters and the solar magnetic cycle by considering the phase of each component and its amplitude evolution. While the time lag of the corotating-stream component shows a very similar behavior to that observed for solar wind parameters, the CME component represents an in-phase component with respect to the solar magnetic cycle, and the slow-wind component is in anti-phase. Therefore, the amplitude modulation of each component could explain the observed time variation of the phase. To further investigate in this direction we plan to include in a future model in-phase and quadrature components to relate their amplitudes modulation to the three solar wind components here analyzed.

Additionally, the time lag between solar wind properties and the Ca II K index is continuously investigated over time using a cross-correlation performed over an 11-year sliding window. The results of this analysis reveal the existence of distinct dynamical regimes characterized by the presence of (at least) two different states, which manifest across different time-lag ranges (Figure 5). In particular, we identify unstable configurations at both small (< 2 yr) and large (> 5 yr) lag values, whereas a relatively stable regime emerges at intermediate lags ($2 - 4$ yr). This dependence of the time lags on the phases of the solar cycles suggests the presence of a bifurcation mechanism, i.e., a physical processes governing the shift of the system between the two time-lag states, in agreement with Carbone et al. (2024). Indeed, it is the combined influence of amplitude fluctuations and periodic forcing that gives rise to the observed time lag between solar magnetic activity and solar wind behavior (Carbone et al. 2024). The magnitude of this time lag is further linked to the characteristic scale of the physical processes driving solar activity (e.g., 11-yr solar cycle, quasi-biennial oscillations, and so on). Hence, the time lag, which is linked to physical processes on different

timescales, can act as a potential bifurcation parameter linking solar activity and solar wind properties, as hypothesized by Reda, Giovannelli, and Alberti (2024). This is the first step to construct a simple dynamical system that can mimic the behavior of the phase coherence among solar activity and solar wind properties, whose stability properties (i.e., its long-term resilience into a specific configuration) depend on the time lag. The observed behavior over time (see Figure 5) suggests the presence of a peculiar type of bifurcation, the so-called pitchfork bifurcation (Strogatz 2024), through which the system moves from a stable configuration (in our case, the synchronization with solar cycle variability) to an unstable one (asynchronous behavior) as a control parameter, in our case the time lag, crosses a critical threshold. This interpretation is confirmed by the behavior of the correlation coefficient, which exhibits non-monotonic variations with lag and shows clear signatures of a transition region. In this framework, the correlation coefficient may be interpreted as a proxy for the local coherence of the system, which follows a specific rule for its time behavior during the stable regime (i.e., a periodic time behavior with the solar cycle phases) and assuming only low or high values in the unstable zones.

In a similar phenomenological approach as that introduced in Alberti et al. (2020) for the analysis of magnetic-field fluctuations in the solar wind, we suggest that the observed structure of stability can be described through an effective potential $V(x;\tau)$, where τ is the lag and x represents a reduced dynamical variable (e.g., fluctuation amplitude or phase coherence). A simplified form of such potential may be written as

$$V(x;\tau) = \frac{1}{2}a(\tau)\,x^2 - \frac{1}{4}x^4 \tag{4}$$

with $a(\tau)$ capturing the lag-dependent stability of the system. Indeed, in its normal form, a system undergoing a subcritical pitchfork bifurcation can be described via (Strogatz 2024)

$$\frac{dx}{dt} = -\frac{\partial V(x;\tau)}{\partial x} = -a(\tau).x + x^3 \tag{5}$$

The sign of $a(\tau)$ determines the nature of the equilibrium: for $a(\tau) > 0$, the system exhibits a single stable state (intermediate lags), while for $a(\tau) < 0$, the potential develops two symmetric minima corresponding to unstable states (small and large lags), separated by an unstable fixed point at the origin. The lag dependence of $a(\tau)$ therefore governs the bifurcation structure and provides a natural interpretation for the observed dynamical transitions. However, in our case the bifurcation parameter not only depends on τ but also on the solar cycle phases, i.e., it depends on time t, thus making our dynamical system a non-autonomous one. Unlike autonomous systems, where the evolution depends only on the current state, non-autonomous systems evolve according to rules that change over time. One of the primary consequences of this is the presence of temporal variability in the dynamics: the vector field that govern the dynamics, i.e., the potential $V(x;\tau)$ is no longer static, then the structure of phase space, such as fixed points, attractors, or stability basins, may vary over time. Closely related to this is the lack of stationarity: the statistical properties of the system may also vary in time, challenging traditional notions of stability, predictability, and recurrence. In particular, it may render long-term forecasts unreliable if the evolution rules themselves are not constant. An additional perspective could also be the possible role of longer timescale processes (i.e., longer than those exploited in our 60 years time series) in determining the temporal behavior of the bifurcation parameters, thus necessarily including additional physical processes (e.g., the Gleissberg cycle with amplitude modulation of solar cycles with a period of about 70 – 100 years) to determine the analytical or parametric

form of $a(\tau)$. Thus, our framework offers a qualitative explanation of our empirical findings, but also allows us to place them in a broader dynamical system's perspective, emphasizing the importance of scale-dependent transitions in heliophysical time series. It also opens the way for quantitative modeling via reduced stochastic differential equations or normal-form analysis to further investigate the nature of the bifurcation and its physical implications.

Acknowledgments We sincerely acknowledge an anonymous reviewer for useful suggestions and comments.

Author Contributions R.R., L.G., and T.A. wrote the main manuscript text. R.R. performed the analysis and prepared all figures with the contribution of L.G. and T.A. . All authors reviewed the manuscript.

Funding Information Open access funding provided by Università degli Studi di Roma Tor Vergata within the CRUI-CARE Agreement. This study was carried out within the Space It Up project funded by the Italian Space Agency, ASI, and the Ministry of University and Research, MUR, under contract n. 2024-5-E.0 - CUP n. I53D24000060005.

R.R. acknowledges the support from the project "Realizzazione di un'Infrastruttura HW e SW (IHS) presso il CGS/Matera (CUP F83C22002460005), in attuazione del Piano Operativo del sub-investimento M1C2.I4.4 'In-Orbit Economy - SST—FlyEye' del PNRR-FC".

Data Availability The authors acknowledge use of NASA/GSFC's Space Physics Data Facility's OMNIWeb service and OMNI data. The Ca II K index composite data are accessible at the SOLIS webpage (https://solis.nso.edu/0/iss/), which is operated by the National Solar Observatory. The Mg II index composite, made available by the University of Bremen, can be accessed at https://www.iup.uni-bremen.de/UVSAT/Datasets/mgii. The classification of near-Earth solar wind structure types is accessible at DOI.

Declarations

Competing Interests The authors declare no competing interests.

References

Alberti, T., Laurenza, M., Consolini, G., Milillo, A., Marcucci, M.F., Carbone, V., Bale, S.D.: 2020, On the scaling properties of magnetic-field fluctuations through the inner heliosphere. *Astrophys. J.* **902**, 84. DOI. ADS.

Beer, J., Tobias, S.M., Weiss, N.O.: 2018, On long-term modulation of the Sun's magnetic cycle. *Mon. Not. R. Astron. Soc.* **473**, 1596. DOI. ADS.

Bertello, L., Pevtsov, A., Tlatov, A., Singh, J.: 2016, Correlation between sunspot number and Ca II K emission index. *Sol. Phys.* **291**, 2967. DOI. ADS.

Carbone, V., Alberti, T., Reda, R., Giovannelli, L.: 2024, Space-climatic feedback of the magnetic solar cycle through the interplanetary space. *Sci. Rep.* **14**, 19850. DOI. ADS.

Dash, S., Nandy, D., Usoskin, I.: 2023, Long-term forcing of the Sun's coronal field, open flux, and cosmic ray modulation potential during grand minima, maxima, and regular activity phases by the solar dynamo mechanism. *Mon. Not. R. Astron. Soc.* **525**, 4801. DOI. ADS.

El-Borie, M.A.: 2002, On long-term periodicities in the solar-wind ion density and speed measurements during the period 1973 – 2000. *Sol. Phys.* **208**, 345. DOI. ADS.

Ferreira, R.R., Gonçalves, B.F.O., do Nascimento, J.-D., Castro, M.: 2024, A correlation between sunspot observations and solar Ca II H&K activity proxies. *Mon. Not. R. Astron. Soc.* **535**, 2394. DOI. ADS.

Hathaway, D.H.: 2010, The solar cycle. *Living Rev. Sol. Phys.* **7**, 1. DOI. ADS.
Hazra, S., Réville, V., Perri, B., Strugarek, A., Brun, A.S., Buchlin, E.: 2021, Modeling solar wind variations over an 11 year cycle with Alfvén wave dissipation: a parameter study. *Astrophys. J.* **910**, 90. DOI. ADS.
Kahil, F., Riethmüller, T.L., Solanki, S.K.: 2017, Brightness of solar magnetic elements as a function of magnetic flux at high spatial resolution. *Astrophys. J. Suppl. Ser.* **229**, 12. DOI. ADS.
Katsavrias, C., Preka-Papadema, P., Moussas, X.: 2012, Wavelet analysis on solar wind parameters and geomagnetic indices. *Sol. Phys.* **280**, 623. DOI. ADS.
King, J.H., Papitashvili, N.E.: 2005, Solar wind spatial scales in and comparisons of hourly wind and ACE plasma and magnetic field data. *J. Geophys. Res. Space Phys.* **110**, A02104. DOI. ADS.
Köhnlein, W.: 1996, Cross-correlation of solar wind parameters with sunspots ('long-term variations') at 1 AU during cycles 21 and 22. *Astrophys. Space Sci.* **245**, 81. DOI. ADS.
Li, K.J., Zhang, J., Feng, W.: 2017, Periodicity for 50 yr of daily solar wind velocity. *Mon. Not. R. Astron. Soc.* **472**, 289. DOI. ADS.
Perri, B., Brun, A.S., Strugarek, A., Réville, V.: 2021, Dynamical coupling of a mean-field dynamo and its wind: feedback loop over a stellar activity cycle. *Astrophys. J.* **910**, 50. DOI. ADS.
Perri, B., Leitner, P., Brchnelova, M., Baratashvili, T., Kuźma, B., Zhang, F., Lani, A., Poedts, S.: 2022, COCONUT, a novel fast-converging MHD model for solar corona simulations: I. Benchmarking and optimization of polytropic solutions. *Astrophys. J.* **936**, 19. DOI. ADS.
Pevtsov, A.A., Virtanen, I., Mursula, K., Tlatov, A., Bertello, L.: 2016, Reconstructing solar magnetic fields from historical observations. I. Renormalized Ca K spectroheliograms and pseudo-magnetograms. *Astron. Astrophys.* **585**, A40. DOI. ADS.
Pinto, R.F., Brun, A.S., Jouve, L., Grappin, R.: 2011, Coupling the solar dynamo and the corona: wind properties, mass, and momentum losses during an activity cycle. *Astrophys. J.* **737**, 72. DOI. ADS.
Reda, R., Giovannelli, L., Alberti, T.: 2023, On the time lag between solar wind dynamic parameters and solar activity UV proxies. *Adv. Space Res.* **71**, 2038. DOI. ADS.
Reda, R., Giovannelli, L., Alberti, T.: 2024, Cross-scale phase relationship of the Ca II K index with solar wind parameters: a space climate focus. *Sol. Phys.* **299**, 105. DOI. ADS.
Reda, R., Penza, V.: 2024, The Ca II K index-Mg II index relation: a Hilbert-Huang transform approach. In: D'Agostino, R., Baldi, A.S., Cacciotto, P., Pietrobon, D., Preziosi, E. (eds.) *12th Young Researcher Meeting, Memorie della Società Astronomica Italiana 95* **46**. DOI. ADS.
Reda, R., Giovannelli, L., Alberti, T., Berrilli, F., Bertello, L., Del Moro, D., Di Mauro, M.P., Giobbi, P., Penza, V.: 2023, The exoplanetary magnetosphere extension in Sun-like stars based on the solar wind-solar UV relation. *Mon. Not. R. Astron. Soc.* **519**, 6088. DOI. ADS.
Reda, R., Stumpo, M., Giovannelli, L., Alberti, T., Consolini, G.: 2024, Disentangling the solar activity-solar wind predictive causality at space climate scales. *Rend. Lincei, Sci. Fis. Nat.* **35**, 49. DOI. ADS.
Reiss, M.A., MacNeice, P.J., Mays, L.M., Arge, C.N., Möstl, C., Nikolic, L., Amerstorfer, T.: 2019, Forecasting the ambient solar wind with numerical models. I. On the implementation of an operational framework. *Astrophys. J. Suppl. Ser.* **240**, 35. DOI. ADS.
Richardson, I.: 2023, Solar Wind Structure List Since 1963, Harvard Dataverse. DOI.
Richardson, I.G., Cane, H.V.: 2012, Near-Earth solar wind flows and related geomagnetic activity during more than four solar cycles (1963 – 2011). *J. Space Weather Space Clim.* **2**, A02. DOI. ADS.
Samsonov, A.A., Bogdanova, Y.V., Branduardi-Raymont, G., Safrankova, J., Nemecek, Z., Park, J.-S.: 2019, Long-term variations in solar wind parameters, magnetopause location, and geomagnetic activity over the last five solar cycles. *J. Geophys. Res. Space Phys.* **124**, 4049. DOI. ADS.
Strogatz, S.H.: 2024, *Nonlinear Dynamics and Chaos: With Applications to Physics, Biology, Chemistry, and Engineering*, Chapman and Hall/CRC, London.
Usoskin, I.G.: 2023, A history of solar activity over millennia. *Living Rev. Sol. Phys.* **20**, 2. DOI. ADS.
Vecchio, A., Lepreti, F., Laurenza, M., Alberti, T., Carbone, V.: 2017, Connection between solar activity cycles and grand minima generation. *Astron. Astrophys.* **599**, A58. DOI. ADS.
Zwiers, F.W., von Storch, H.: 1995, Taking serial correlation into account in tests of the mean. *J. Clim.* **8**, 336. DOI. ADS.